

# Emodin Ameliorates Severe Acute Pancreatitis-Associated Acute Lung Injury in Rats by Modulating Exosome-Specific miRNA Expression Profiles

Qi Yang<sup>1-4</sup>, Yalan Luo<sup>1-3</sup>, Peng Ge<sup>1-3</sup>, Bowen Lan<sup>1-3</sup>, Jin Liu<sup>1-3</sup>, Haiyun Wen<sup>1-3</sup>, Yinan Cao<sup>1-3</sup>, Zhenxuan Sun<sup>1-3</sup>, Guixin Zhang<sup>1-3</sup>, Huiming Yuan<sup>5</sup>, Lihua Zhang<sup>5</sup>, Hailong Chen<sup>1-3</sup>

<sup>1</sup>Department of General Surgery, the First Affiliated Hospital of Dalian Medical University, Dalian, Liaoning, 116011, People's Republic of China; <sup>2</sup>Institute (College) of Integrative Medicine, Dalian Medical University, Dalian, Liaoning, 116011, People's Republic of China; <sup>3</sup>Laboratory of Integrative Medicine, the First Affiliated Hospital of Dalian Medical University, Dalian, Liaoning, 116011, People's Republic of China; <sup>4</sup>Department of Traditional Chinese Medicine, the Second Affiliated Hospital of Dalian Medical University, Dalian, 116023, People's Republic of China; <sup>5</sup>CAS Key Laboratory of Separation Science for Analytical Chemistry, National Chromatographic Research and Analysis Center, Dalian Institute of Chemical Physics, Chinese Academy of Science, Dalian, 116023, People's Republic of China

Correspondence: Hailong Chen, Email [chenhailong@dmu.edu.cn](mailto:chenhailong@dmu.edu.cn)

**Background:** Numerous preclinical investigations have exhibited the beneficial impact of emodin (EMO) on the management of severe acute pancreatitis (SAP)-associated acute lung injury (ALI). However, the potential of EMO to mitigate organ damage through the modulation of exosome (Exo)-specific miRNA expression profiles remains unclear.

**Methods:** The SAP rat model was established by retrograde injection of 5% sodium taurocholate into the pancreatic bile duct. Rats received intragastric administration of EMO at 2 h and 12 h post-modeling. Plasma and bronchoalveolar lavage fluid (BALF)-derived exosomes were isolated and purified from SAP rats treated with EMO. The therapeutic effects of these Exos in SAP rats were assessed using hematoxylin-eosin staining and measurement of inflammatory factor levels. MicroRNA (miRNA) sequencing was conducted on plasma and BALF-derived Exos, and rescue experiments were performed to investigate the function of NOVEL miR-29a-3p in the treatment of SAP using EMO.

**Results:** EMO exhibits ameliorative effects on pancreatic and lung injury and inflammation in rats with SAP. Plasma/BALF-derived Exos from EMO-treated SAP rats also have therapeutic effects on SAP rats. The miRNA expression profile of plasma and BALF-derived Exos in SAP rats underwent significant changes upon exposure to EMO. In particular, 34 differentially expressed miRNAs (DEmiRNAs) were identified when comparing BALF-SAP+EMO-Exo and BALF-SAP-Exo. 39 DEmiRNAs were identified when comparing plasma-SAP+EMO-Exo to plasma-SAP-Exo. We found that SAP rats treated with Exos derived from BALF exhibited a more potent therapeutic response than those treated with Exos derived from plasma. EMO may rely on NOVEL-rno-miR-29a-3p expression to prevent pulmonary injury in SAP rats.

**Conclusion:** The mechanism of action of EMO is observed to have a significant impact on the miRNA expression profile of Exos derived from plasma and BALF in SAP rats. NOVEL-rno-miR-29a-3p, which is specific to Exos, and is derived from BALF, may play a crucial role in the therapeutic efficacy of EMO.

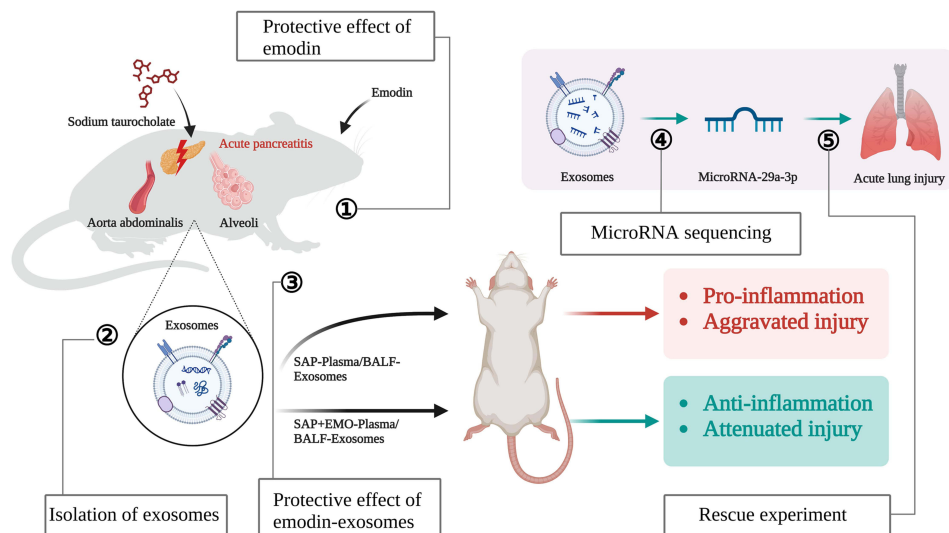
## Plain Language Summary:

- Exosomes extracted from plasma/BALF of EMO-treated SAP rats show a substantial therapeutic impact on SAP-Associated ALI, with BALF-derived exosomes having a higher therapeutic effect than plasma-derived exosomes.
- EMO dramatically altered the miRNA expression patterns of plasma and BALF-derived exosomes in SAP rats.
- The lung protective effect of EMO in SAP rats is somewhat reliant on Novel-rno-miR-29a-3p expression.

**Keywords:** severe acute pancreatitis, acute lung injury, emodin, exosome, microRNA

## Graphical Abstract

### Emodin Ameliorates Severe Acute Pancreatitis-Associated Acute Lung Injury in Rats by Modulating Exosome-Specific MiRNA Expression Profiles



## Introduction

Acute pancreatitis (AP) is a common inflammatory illness of the digestive system, with approximately 20% of patients progressing to severe acute pancreatitis (SAP), with a mortality rate of 20%.<sup>1</sup> The mortality rate of patients with SAP exhibits bimodal distribution with two distinct peaks.<sup>2</sup> The first peak occurs during the initial stage of the disease, typically within 1–2 weeks of onset, and is characterized by aseptic inflammation, systemic inflammatory response syndrome (SIRS), and multiple organ dysfunction syndrome (MODS). The second peak occurs during the advanced stage of the disease, which typically manifests around two weeks after onset. SAP patients develop infectious pancreatic necrosis during this stage, which may be accompanied by sepsis and MODS.<sup>2</sup> It is imperative to underscore that acute lung injury (ALI)-induced respiratory failure represents the most prevalent form of organ dysfunction and the main reason for the bimodal distribution of mortality in SAP patients.<sup>3</sup> Currently, there exists no targeted treatment for SAP-associated ALI. The efficacy of symptomatic treatments, such as infection management and enhancement of respiratory function, is suboptimal. It is imperative to investigate efficacious treatment modalities specific to SAP-associated ALI.

Extracellular vesicles (EVs) have emerged as a highly active area of research in the past decade.<sup>4</sup> Exosomes (Exos) is a type of EVs characterized by a particle size that falls between 40 to 160 nm. Most cells can actively release Exos that contain various cargoes such as nucleic acids, lipids, phospholipid bilayers, proteins, and metabolites. Exos are ubiquitous in multiple bodily fluids and play a crucial role in intercellular communication by facilitating the transfer of biomolecules—the vast majority of Exos transport microRNAs (miRNAs).<sup>5</sup> Two wrongs may balance out a right. Previously, miRNAs and Exos were considered byproducts with no significant biological function in living organisms. The amalgamation of Exos and microRNAs exhibits substantial potential in translational medicine. Exo-specific miRNAs obtained from serum, plasma, and ascites significantly impact the onset and progression of SAP by modulating post-transcriptional modification and inflammatory cell signaling. Exo-specific miRNAs also have the potential to serve as diagnostic markers and therapeutic agents for SAP.<sup>6</sup>

Emodin (EMO) is an anthraquinone derivative that is abundantly present in *Rheum palmatum* L., *Polygonum multiflorum* Thunb., and *Polygonum cuspidatum* Siebold & Zucc.<sup>7</sup> The solubility characteristics of EMO indicate that it is soluble in alcohol and alkali solutions while exhibiting almost negligible solubility in water. Well-established

techniques exist for emodin extraction, encompassing organic solvent and acid-base extraction. Thus, EMO presents a cost-effective option that does not entail a significant financial strain on individuals seeking treatment.<sup>8</sup> EMO displays various pharmacological properties, such as anti-inflammatory, antioxidant, anti-fibrotic, purgative, hemostatic, hypoglycemic, and antibacterial effects.<sup>8</sup> Numerous preclinical investigations have exhibited the beneficial impact of EMO on the management of SAP. The etiology of ALI caused by SAP is multifaceted, encompassing various mechanisms, including pancreatic microcirculation disorder, impairment of intestinal barrier function, the interplay of inflammatory cascade signaling pathways, and destruction of the pulmonary air-blood barrier. According to reports, EMO can inhibit the intercommunication of inflammatory cascade signals, intestinal barrier injury, disruption of microcirculation, programmed cell death of parenchymal cells, and damage to extrapancreatic organs, particularly in managing ALI.<sup>9</sup> Our team has previously elucidated the regulatory mechanism underlying the beneficial effects of EMO on SAP-associated ALI through the utilization of proteomic and transcriptomic methodologies.<sup>10,11</sup> However, the potential of EMO to mitigate organ damage through the modulation of Exo-specific miRNA expression profiles remains unclear.

The present investigation involved the isolation of Exos from plasma/bronchoalveolar lavage fluid (BALF) obtained from SAP rats undergoing EMO treatment and the subsequent evaluation of their therapeutic efficacy in SAP rats. The regulatory mechanisms of EMO therapy for SAP were further elucidated through miRNA sequencing and rescue experiment.

## Materials and Methods

### Reagents and Instruments

Emodin (EMO) and sodium taurocholate (STC) were purchased from Sigma. Hematoxylin-eosin (HE) staining kit and immunohistochemistry (IHC) staining kit were purchased from Servicebio. Isoflurane was purchased from RWD. Tumor necrosis factor- $\alpha$  (TNF- $\alpha$ ), interleukin-1 $\beta$  (IL-1 $\beta$ ), and IL-6 kits were purchased from Elabscience. Amylase kit purchased from Nanjing Jiancheng. Exosome special protein lysate was purchased from Umibio. The real-time quantitative PCR (RT-qPCR) primer, antago-negative control (NC), and antago-NOVEL-miR-29a-3p were synthesized by GenePharma. A primary antibody against tumor susceptibility gene 101 (TSG101) was purchased from HUABIO. A primary antibody against Ly6G was purchased from Affinity. A primary antibody against CD81, CD63, or inducible nitric oxide synthase (iNOS) was purchased from Abclonal. A primary antibody against Calnexin was purchased from Affinity. Anesthesia machine purchased from RWD. The optical microscope was purchased from Olympus. Electrophoresis equipment was purchased from the BIO-RAD. The automatic microplate reader was purchased from BioTek.

### Animal Grouping and Treatment

The male Sprague-Dawley (SD) rats utilized in the study were procured from Liaoning Changsheng Biotechnology Co., LTD. and were housed at the Animal Laboratory Center of Dalian Medical University. The animal experiments are approved by the Experimental Animal Ethics Review Committee of Dalian Medical University (Ethics number AEE19003) and adhere to the National Institutes of Health (USA)'s Guidelines for the Care and Use of Experimental Animals. A total of 128 SD rats of the SPF grade, aged 8 weeks and exhibiting a body mass within the range of 200 to 220 g, were selected for the study. The feeding conditions were as follows: a relative humidity of 50%  $\pm$  1%, a temperature of (24  $\pm$  1)  $^{\circ}$ C, and a light-dark cycle of 12 h per day. All the rats were provided with ad libitum access to food and water. Before the modeling procedure, the rats underwent a period of fasting and water consumption for a duration of 12 h. The rats were anesthetized with isoflurane, and the pancreaticoduodenum was isolated into the medial part of the duodenum after disinfection and laparotomy. Subsequently, the SAP rat model was established by retrograde pumping 5% STC (0.1 mL/kg) into the pancreatic bile duct. The sham-operated (SO) group was administered an equivalent saline solution.

Rats received intragastric administration of EMO at 2 h and 12 h (40 mg/kg body weight) post-modeling for treatment.<sup>10</sup> Plasma and BALF were obtained from rats in the SAP and EMO groups after 24 h of modeling, and Exos was isolated. Regarding the treatment regimen of Exos in SAP rats, we made the necessary modifications to the

dosage described in previous literature to administer Exos (0.25 mg protein/kg body weight, intratracheal instillation) at 2 h and 12 h following modeling.<sup>12</sup> 2 and 12 h after modeling. Rats were administered antago-NOVEL-rno-miR-29a-3p and -NC (5 nmol, intratracheal instillation) in the third series of animal experiments.<sup>13</sup> Samples of plasma, pancreatic tissue, lung tissue, and bronchoalveolar lavage fluid were collected after 24 h of modeling.

## Rat Living Conditions Observation

We observed the rats' living conditions at 6, 12, and 24 h after modeling. The observations included changes in body mass, expression, fur luster and shedding, and stool characteristics for each rat.

## Histopathological Examination and Immunohistochemistry

The fresh lung and pancreatic tissues were soaked in a solution of 4% paraformaldehyde for fixation, followed by paraffin embedding and sectioning into 4 $\mu$ m thickness. Following the dewaxing and dehydration procedures, the tissue sections were subjected to hematoxylin-eosin staining (HE) staining and subsequently examined for pathological alterations in the pancreatic and lung tissues using an optical microscope.<sup>14</sup> After the dewaxing and antigen repair procedures, the sections were subjected to the endogenous enzyme and serum blocking. Subsequently, the primary antibody was applied and incubated overnight at 4 °C, followed by incubation with the secondary antibody at 37 °C for 1 h on the following day. The specimens underwent a series of procedures, including color development through using 3,3-N-Diaminobenzidine Tetrahydrochloride, hematoxylin counterstaining, dehydration, and final sealing and photographic documentation.

## Determination of Plasma Amylase Activity and Inflammatory Factors

The collected blood samples were left for 2 h and centrifuged at 3000 rpm for 10 min to obtain plasma. The activity of amylase in plasma was determined by iodine-starch colorimetry. According to the kit instructions, the enzyme-linked immunosorbent assay (ELISA) method detected the expression levels of inflammatory cytokines IL-6, IL-1 $\beta$ , and TNF- $\alpha$  in plasma.

## Measurement of Lung Tissue Wet-Dry Weight (W/D) Ratio

The fresh left lung of each group was clipped, cleansed of surface blood with phosphate buffer saline, dried with filter paper, and weighed to record its wet weight. Then, the left lung was dehydrated at a constant temperature of 70 °C for 48 h until it reached a constant weight. The dry weight was measured and used for calculating the W/D ratio.

## Blood Gas Analysis

Arterial blood was collected from the abdominal aorta using heparin sodium-rinsed 1 mL syringe. The collected blood was immediately analyzed for arterial partial pressure of oxygen (PaO<sub>2</sub>) and partial pressure of carbon dioxide (PaCO<sub>2</sub>) using an automatic blood gas analyzer.

## Quantification of Protein in BALF

The BALF was centrifuged at 4°C and 12000 rpm for 10 min. The optical density of the collected supernatant was measured using the bicinchoninic acid assay (BCA) kit protocol. According to the standard curve, the total protein concentration in BALF was calculated.

## Isolation and Characterization of Plasma/BALF-Derived Exos

The plasma and BALF specimens were centrifugated at 4 °C and 2000 $\times$ g for 30 min. The resultant residue was eliminated, and the supernatant was carefully transferred to a fresh centrifuge tube. The supernatant was centrifugated at a temperature of 4 °C and a force of 10,000 $\times$ g for 45 min. Subsequently, the resulting supernatant was collected and filtered through a 0.45 $\mu$ m filter membrane. The obtained filtrate was subjected to centrifugation at a temperature of 4 °C and a force of 100 000 $\times$ g for 70 min. After removing the supernatant, the remaining pellets was reconstituted with 10 mL of pre-cooled 1 $\times$ PBS and subjected to a second round of centrifugation lasting 70 min. The liquid portion of the sample

was extracted, and the Exos were obtained using 500  $\mu$ L of pre-cooled 1 $\times$ PBS re-suspended precipitation. Exos were extracted from a 10  $\mu$ L sample and subsequently characterized using a transmission electron microscope (TEM). The NanoSight NS300 was utilized to conduct nanoparticle tracking analysis (NTA). The identification of exosomal markers was carried out through Western Blot analysis, as described in 2.14.

## Observation of Lung Ultrastructure

The lung tissues of 2 mm $\times$ 2 mm $\times$ 2 mm were taken from the rats within 1–3 min and fixed in 2.5% glutaraldehyde solution for 48 h. The ultrastructure changes of the lung tissues, including lamellar bodies, microvilli, and tight junctions, were observed by TEM.

## MicroRNA Sequencing

The TRIzol method was utilized to extract total RNA from Exos, followed by miRNA sequencing conducted by LC-Bio Technologies (Hangzhou) CO., LTD. The experimental protocols were executed by the established procedures outlined by Illumina, which encompassed the preparation of libraries and the sequencing experiments.

## Screening and qRT-PCR Verification of Differentially Expressed miRNAs (DEmiRNAs)

Principal component analysis (PCA) was conducted utilizing the gene expression profile of six samples. By employing PCA as a technique for dimensionality reduction, it becomes possible to more directly observe the relationship and variation between models in the data. The present study used screening criteria based on Fold change (FC) values exceeding 1.2 or less than 0.83 and a p-value threshold of less than 0.05. To depict miRNAs that exhibit significant variations between groups, log<sub>2</sub> FC was employed as the x-axis, while the -log<sub>10</sub> p-value was used as the y-axis to generate a volcano plot of miRNA expression.

The TRIzol method was utilized to extract total RNA from Exos. RNA purity and content were detected, and reverse transcription was performed according to kit instructions. A 20  $\mu$ L PCR reaction system was prepared with an RT-qPCR kit. The test was repeated three times for a single sample. After the amplification reaction, the melting curve analysis was performed to determine whether the product had non-specific amplification. The amplification curve was analyzed, the Ct value was calculated, and the relative quantitative analysis was performed by the  $2^{-\Delta\Delta C_t}$  method with U6 as the internal reference. The primers are shown in [Supplementary Table S1](#).

## Prediction and Functional Enrichment Analysis of Target Genes of DEmiRNAs

TargetScan and miRanda were utilized to predict the target genes of DEmiRNAs. During the TargetScan screening process, genes with a context score percentile lower than 50 were eliminated. During the miRanda screening process, genes with maximum free energy exceeding -10 were eliminated. Ultimately, the final set of target genes for DEmiRNAs was determined by identifying the intersection between TargetScan and Miranda-screened data.

The Gene Ontology (GO) analysis provides a comprehensive annotation for describing the functional attributes of genes, encompassing their molecular function (MF), cellular component (CC), and biological process (BP). The Kyoto Encyclopedia of Genes and Genomes (KEGG) employs a pathway-centric approach to gene classification, whereby genes with similar functions are organized into distinct pathways. The GO and KEGG enrichment analysis was utilized to enrich the target genes of DEmiRNAs, and subsequently, bubble maps and histogram were generated.

## Western Blotting

Protein extraction from Exos derived from plasma or BALF was carried out using a lysate specific to exosomal proteins. The crude protein sample underwent centrifugation at a temperature of 4°C and a speed of 10,000 rpm for 10 min. The resulting supernatant was collected, and its concentration was determined using the BCA method. Subsequently, an equivalent quantity of protein that is specific to Exos was isolated through the process of electrophoresis on a gel made of polyacrylamide and sodium dodecyl sulfate. The protein is transferred onto the polyvinylidene fluoride (PVDF) membrane and subsequently blocked with a 5% skim milk solution. Antibodies CD63, CD81, TSG101, and Calnexin were introduced and subjected to an overnight incubation at a temperature of 4°C. On a subsequent day, the PVDF

membrane was incubated with the secondary antibody for 2 h at ambient temperature. The PVDF membrane was subjected to ultra-sensitive ECL luminescent solution, exposure, and photography in the gel imaging system.

## Statistical Analysis

The statistical analysis was conducted using the SPSS 24.0 software. The data obtained from the measurements were presented as mean  $\pm$  standard deviation. The comparison between the two groups was conducted using the Student's *t*-test. We used a one-way analysis of variance (ANOVA) to assess the differences between the three or more groups. Additionally, Fisher's least significant difference (LSD) was used as post hoc after ANOVA. When the *p*-value is less than 0.05, it suggests a significant statistical difference.

## Results

### Emodin Exhibits Ameliorative Effects on Pancreatic and Lung Injury and Inflammation in Rats with SAP

Figure 1A displays the experimental design and animal treatment. The male adult rats were randomly assigned to three groups: SO, SAP, and SAP+EMO. We observed the general status of each group of rats. The survival status of rats in the SAP group remained normal at 6 h, and there was no significant change compared with that in the SO group. After 12 h of modeling, the condition of the SAP rats deteriorated, as evidenced by decreased activity, disheveled hair, and moderate abdominal swelling. At 24 h, rats with SAP exhibited signs of pain, stress, lethargy, significant abdominal distension, and emaciation. The SAP+EMO group showed more excellent survival status compared to the SAP group at both 12 and 24 h. The pancreatic tissue of the SAP group exhibited significant cell necrosis, severe edema, and inflammatory cell infiltration when compared to the Sham group (Figure 1B). Additionally, the pulmonary tissue of the SAP group displayed inflammatory cell infiltration and thickening of the alveolar septum (Figure 1B). Amylase is a frequently employed indicator in the clinical diagnosis of SAP. Our findings indicate that amylase activity was elevated by over threefold in the SAP group (Figure 1C). The PaO<sub>2</sub> of the SAP group was lower than that of the SO group, and the PaCO<sub>2</sub> was higher than that of the normal group, as indicated in Figure 1D. The study measured the total protein concentration in BALF and found a significant increase in rats with SAP, as shown in Figure 1E. The SAP group exhibited damage to alveolar type II epithelial cells, mitochondrial swelling and cavitation, and vacuolation of lamellar corpuscles, in comparison to the SO group (Figure 1F). EMO exhibits therapeutic efficacy in SAP rats. The observed outcomes included reduced pancreatic and lung injury, lowered amylase activity, decreased total protein concentration in BALF, improved respiratory function. (Figure 1B-E).

### EMO Reduces the Systemic Inflammatory Response in SAP Rats

We examined the expression of Ly6G in pancreatic and lung tissues. EMO significantly reduced Ly6G positivity in pancreatic and lung tissue, suggesting reduced neutrophil infiltration (Figure 2A). iNOS is one of the indicators of M1-type macrophages. We employed the IHC technique to find that iNOS expression in pancreatic and lung tissues of rats in the SAP group was significantly higher than in the SO group, suggesting that many M1-type macrophages resided in the tissues. However, the expression of iNOS was dramatically decreased by EMO (Figure 2B). The plasma levels of IL-6, IL-1 $\beta$ , and TNF- $\alpha$  established markers of systemic inflammatory response resulting from SAP, notably increased in rats in the SAP group. In contrast, EMO effectively suppressed the increase of inflammatory factors in circulating blood induced by SAP (Figure 2C).

### Characterization of Exos Derived From Plasma and BALF

The Exos isolated from BALF and plasma in the SAP group and SAP+EMO group were identified. The isolated Exos displayed a traditional round and "saucer-like" shape under TEM (Figure 3A and B). TSG101, CD81, and CD63 are exosomal surface protein indicators. Western blot findings demonstrated that the markers above were substantially expressed in both plasma/BALF-derived Exos (Figure 3C and D). Calnexin is an endoplasmic reticulum marker protein and one of the negative indicators of Exos. No Calnexin was found in the extracted Exos (Figure 3C and D), showing

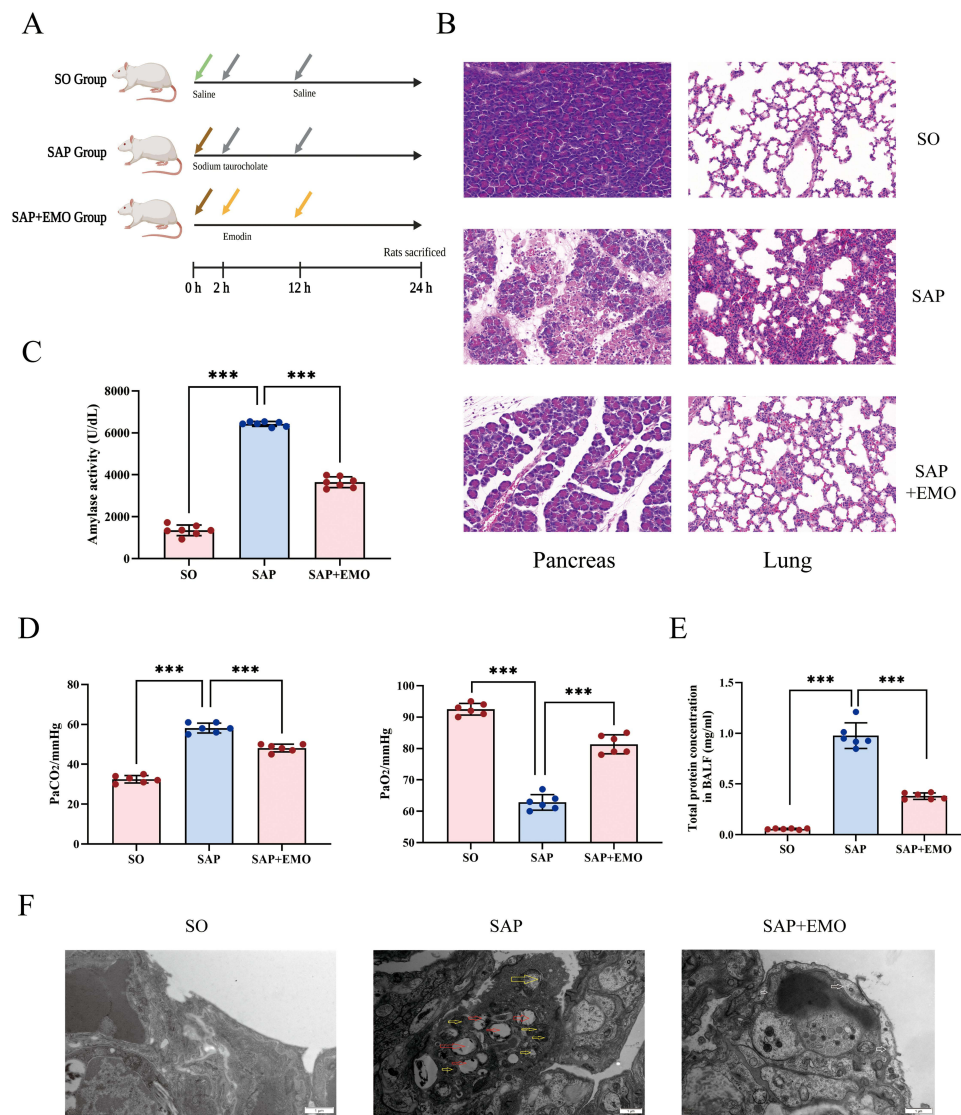


**Figure 1** Emodin exhibits ameliorative effects on pancreatic and lung injury and inflammation in rats with SAP. (A) The experimental design and animal treatment. Created with BioRender.com. (B) HE staining of pancreatic and lung tissue sections (scale bar = 50  $\mu$ m). (C) Plasma amylase activity in rats. (D) Arterial blood gas analysis. (E) Total protein concentration in bronchoalveolar lavage fluid. (F) Observation of ultrastructure of lung tissue in rats. The data consisted of representative images from a minimum of three independent experiments or were presented as mean  $\pm$  standard deviation for each group of rats ( $n = 6$ ). Yellow arrows represent mitochondrial swelling and cavitation, red arrows indicate lamellar bodies, and the white arrow indicates the air-blood barrier. \*\*\*Denotes  $p$ -value < 0.001.

great purity of the extracted Exos. NTA findings indicated that the isolated Exos exhibited a peak particle size of 30–150 nm (Figure 3E and F).

## Plasma/BALF-Derived Exos From EMO-Treated SAP Rats Have Therapeutic Effects on SAP Rats

Our experimental design and animal treatment are depicted in Figure 4A. We observed that plasma-SAP-Exo might enhance SAP-induced lung damage in rats and also validated the inhibitory impact of plasma-SAP +EMO-Exo on SAP-induced lung injury and inflammatory response in rats (Figure 4B-E). Further, we examined the therapeutic impact of BALF-SAP+EMO-Exo on SAP rats. BALF is the fluid of the alveolar surface obtained following the lavage of lung segments and lung subsegments, which possesses lung specificity compared with plasma. We discovered that BALF-SAP-Exo aggravated lung damage and inflammatory response in SAP rats, whereas BALF-SAP+EMO-Exo dramatically reduced SAP-induced lung tissue edema and inflammatory cell infiltration (Figure 4B-E). Interestingly, our data

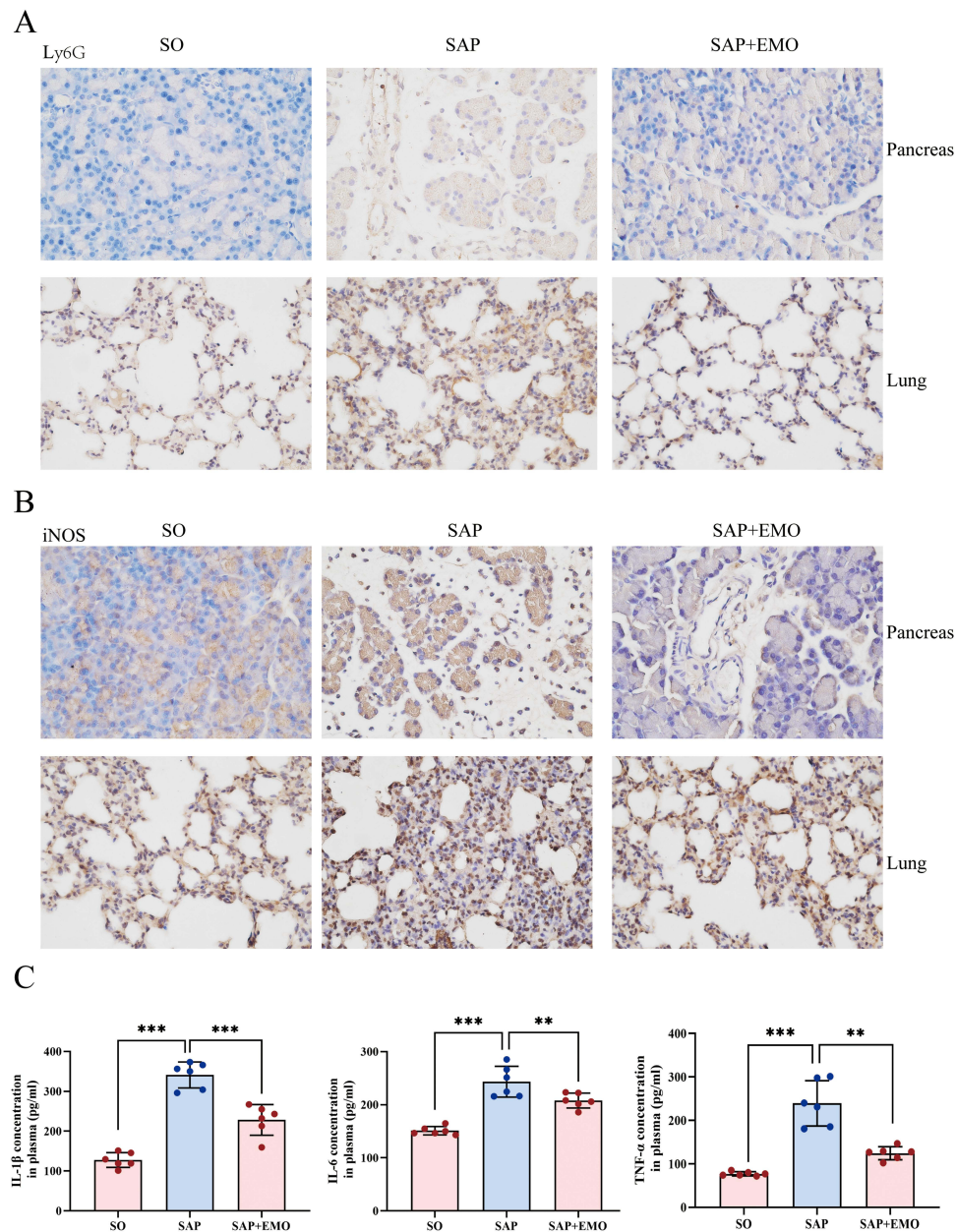


**Figure 2** Emodin reduces the infiltration of macrophages and neutrophils in pancreatic and lung tissues of SAP rats. Immunohistochemical analysis of Ly6G (**A**) and iNOS (**B**) expression in pancreas and lung (scale bar = 20  $\mu$ m). (**C**) Expression levels of TNF- $\alpha$ , IL-6 and IL-1 $\beta$  in rat plasma. The data consisted of representative images from a minimum of three independent experiments or were presented as mean  $\pm$  standard deviation for each group of rats ( $n = 6$ ). \*\* denotes  $p$ -value < 0.01; \*\*\* denotes  $p$ -value < 0.001.

demonstrate that BALF-SAP+EMO-Exo has a more significant therapeutic impact than plasma-SAP+EMO-Exo, which is primarily shown by the downregulation of protein in BALF, as well as improvements in respiratory function and pulmonary edema (Figure 4B-E).

## miRNA Sequencing and Comprehensive Analysis of BALF-Derived Exos

In light of the opposite therapeutic effect of BALF-SAP+EMO-Exo and BALF-SAP-Exo on SAP rats, we followed the standard procedures given by Illumina to produce the library and sequencing tests. Illumina HiSeq 2500 was used to sequence miRNA expression patterns in BALF-SAP+EMO-Exo and BALF-SAP-Exo. miRNA is largely evolutionarily conserved throughout diverse organisms. Based on the discovered miRNAs, we further conducted the length and

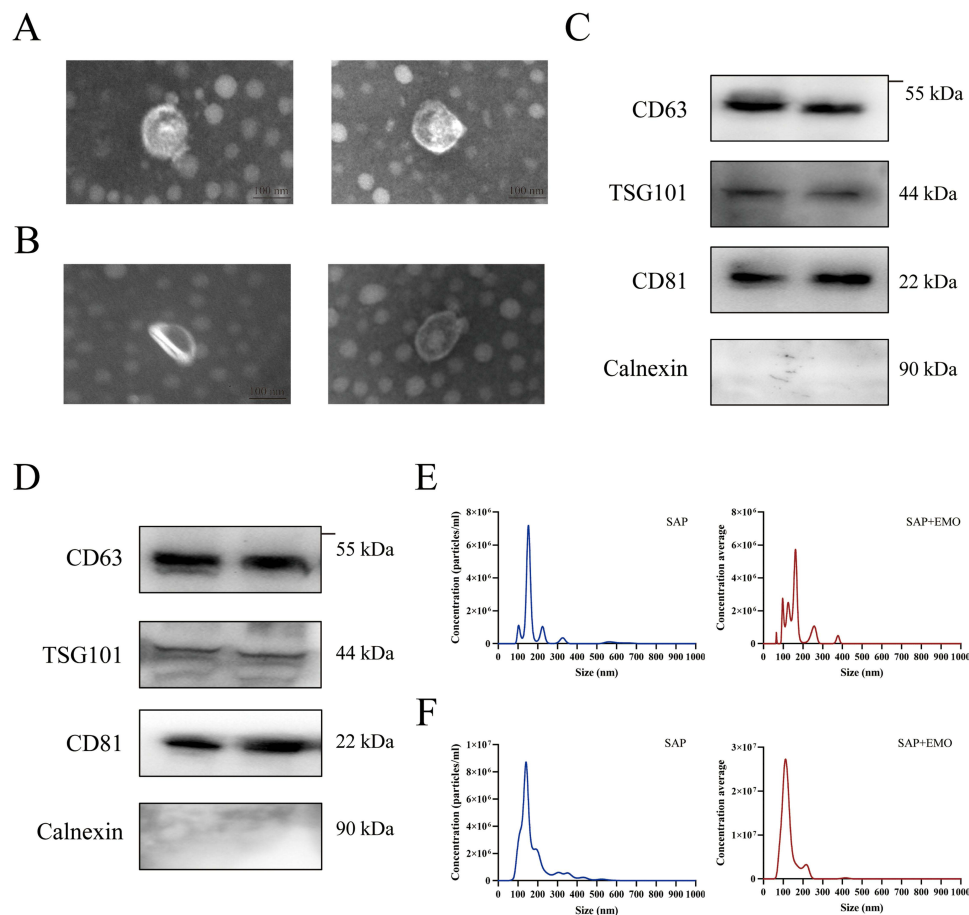


**Figure 3** Characterization of exosomes derived from plasma and BALF. Observation of exosomes derived from plasma (**A**) and BALF (**B**) by transmission electron microscopy. Western blot detection of positive protein CD63, TSG101, CD81, and negative protein Calnexin in exosomes derived from plasma (**C**) and BALF (**D**). Size and concentration of exosomes derived from plasma (**E**) and BALF (**F**) by nanoparticle tracking analysis. bar: 100 nm.

conservative analysis of miRNAs for the chosen species, as shown in [Figure 5A-B](#). The abscissa denotes distinct species, while the ordinate indicates the number of times a precursor has happened in that species. In our following study, only miRNAs from rats were included. PCA findings indicated that there was a substantial gap between the BALF-SAP+EMO-Exo and BALF-SAP-Exo groups in the two-dimensional coordinate system, suggesting variations in miRNA expression patterns between the two groups ([Figure 5C](#)). A Fold change (FC) greater than 1.2 or a Fold change less than 0.83 and P value less than 0.05 were the thresholds for inclusion of DE miRNAs. A total of 34 DE miRNAs were identified, as shown in [Figure 5D-E](#). MiRNAs often form RNA-induced silencing complexes through complementary pairing with the 3'-UTR of target genes, thereby reversely regulating the expression of target genes. We used TargetScan and miRanda to predict the target genes of DE miRNAs, respectively. The intersection of TargetScan and miRanda's prediction serves as the final target gene of DE miRNAs. [Figure 5F-G](#) displays GO/KEGG enrichment analysis finding for potential target genes of DE miRNAs.

## miRNA Sequencing and Comprehensive Analysis of Plasma-Derived Exos

Similarly, we utilized the same approach to evaluate miRNA expression patterns in plasma-SAP+EMO-Exo against plasma-SAP-Exo. [Figure 6A-B](#) illustrates the length and conserved analysis of plasma-derived exosomal miRNAs. In our subsequent investigation, only miRNAs from rats were included. PCA findings indicated that there was a considerable distance between the samples of BALF-SAP+EMO-Exo and BALF-SAP-Exo groups ([Figure 6C](#)). A Fold change (FC) greater than 1.2 or a Fold change less than 0.83 and P value less than 0.05 were the thresholds for inclusion of DE miRNAs. A total of 39 DE miRNAs are discovered, as illustrated in [Figure 6D-E](#). We employed TargetScan and

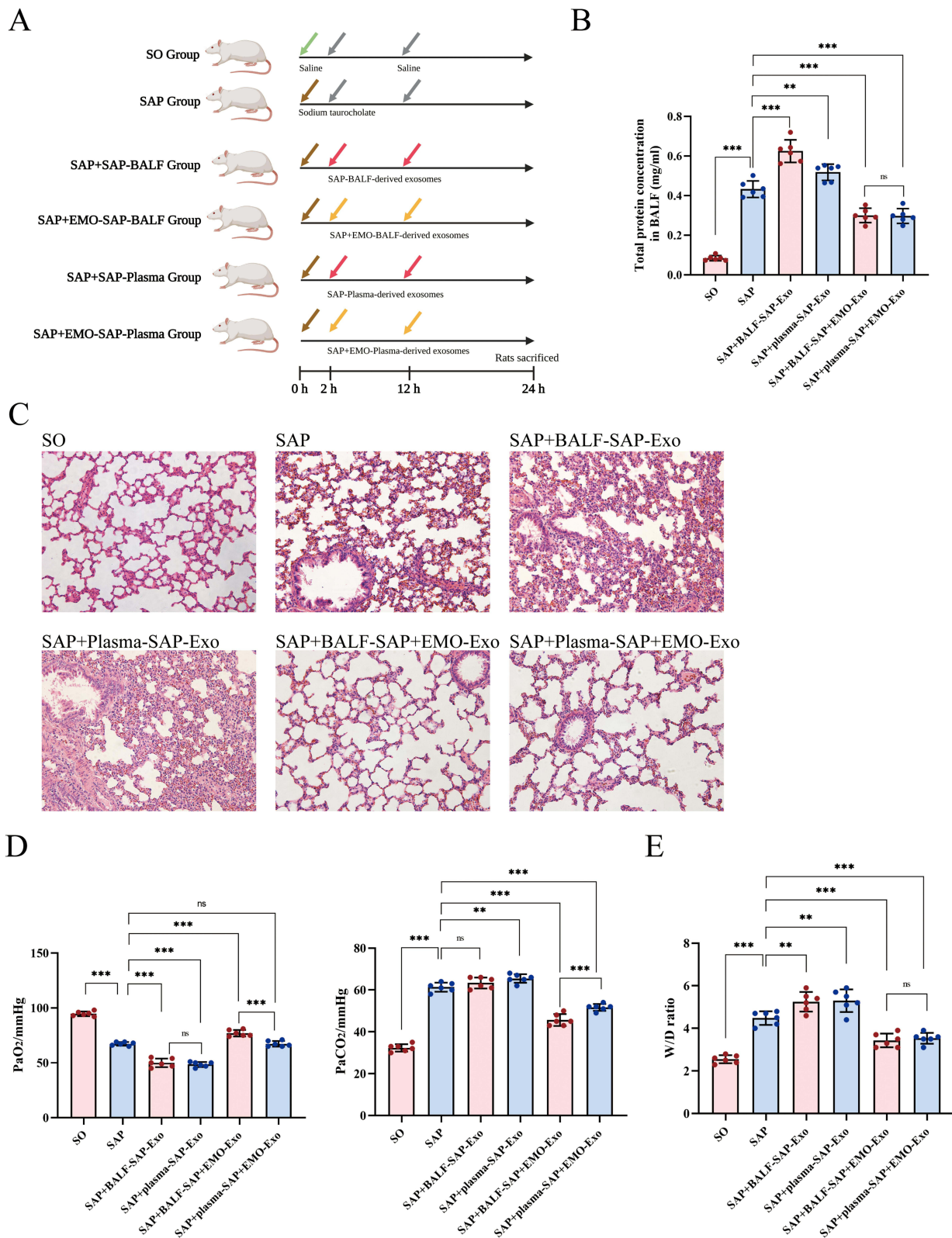


**Figure 4** Plasma/BALF-derived exosomes from EMO-treated SAP rats have therapeutic effects on SAP rats. **(A)** The experimental design and animal treatment. Created with BioRender.com. **(B)** Total protein concentration in bronchoalveolar lavage fluid. **(C)** HE staining of lung tissue sections (scale bar = 50  $\mu$ m). **(D)** Arterial blood gas analysis. **(E)** Wet-dry ratio of rat lung tissue. The data consisted of representative images from a minimum of three independent experiments or were presented as mean  $\pm$  standard deviation for each group of rats ( $n = 6$ ). ns denotes no significance; \*\* denotes p-value < 0.01; \*\*\*Denotes p-value < 0.001.

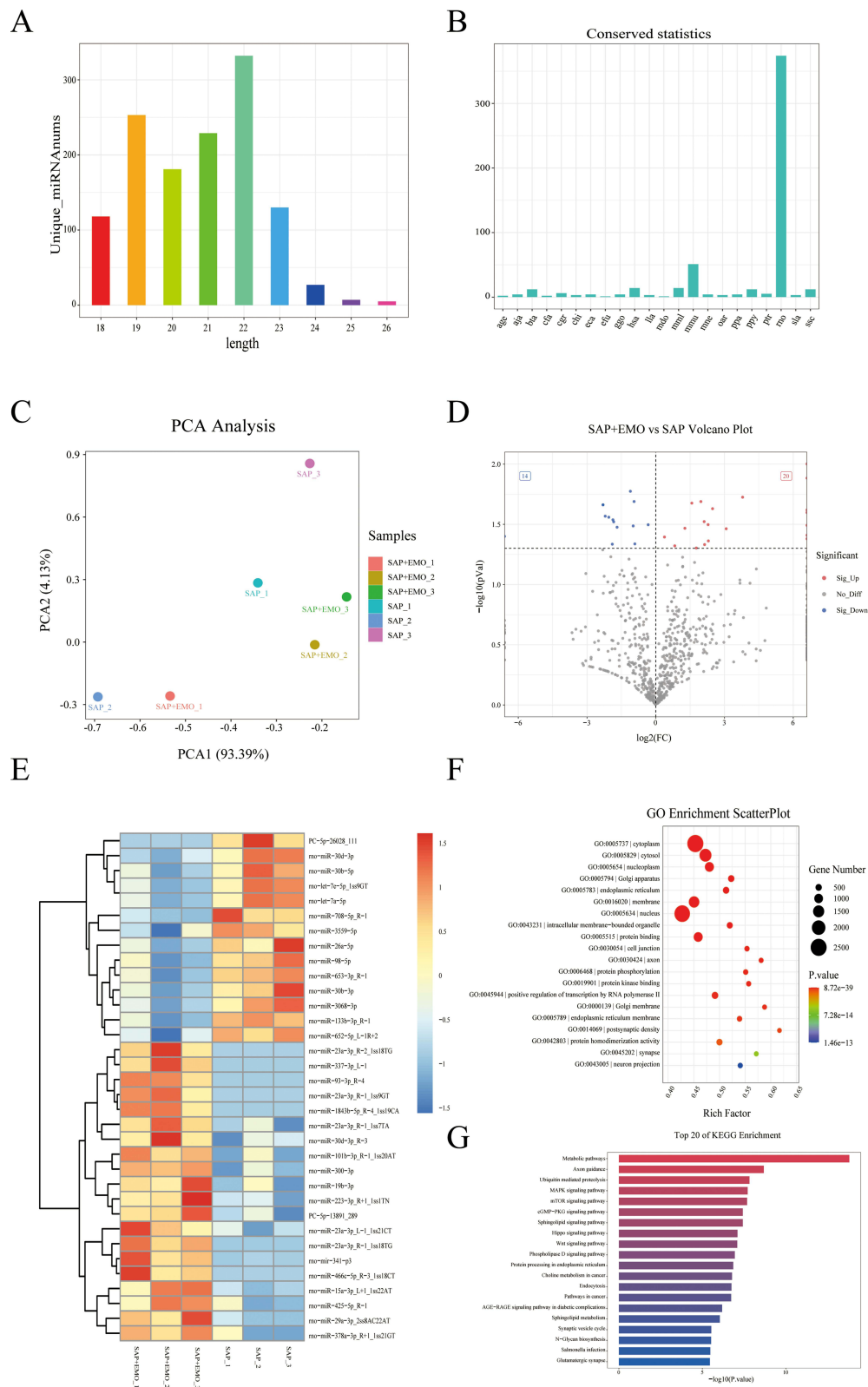


**Figure 5** miRNA sequencing and comprehensive analysis of BALF-derived exosomes. **(A and B)** The length and species conservative analysis of miRNAs. **(C)** Principal component analysis. Volcano plot of differentially expressed miRNAs (DEmiRNAs). **(E)** Clustering heat map of DE miRNAs. **(F)** GO functional enrichment analysis of DE miRNAs target genes. **(G)** KEGG functional enrichment analysis of DE miRNAs target genes.

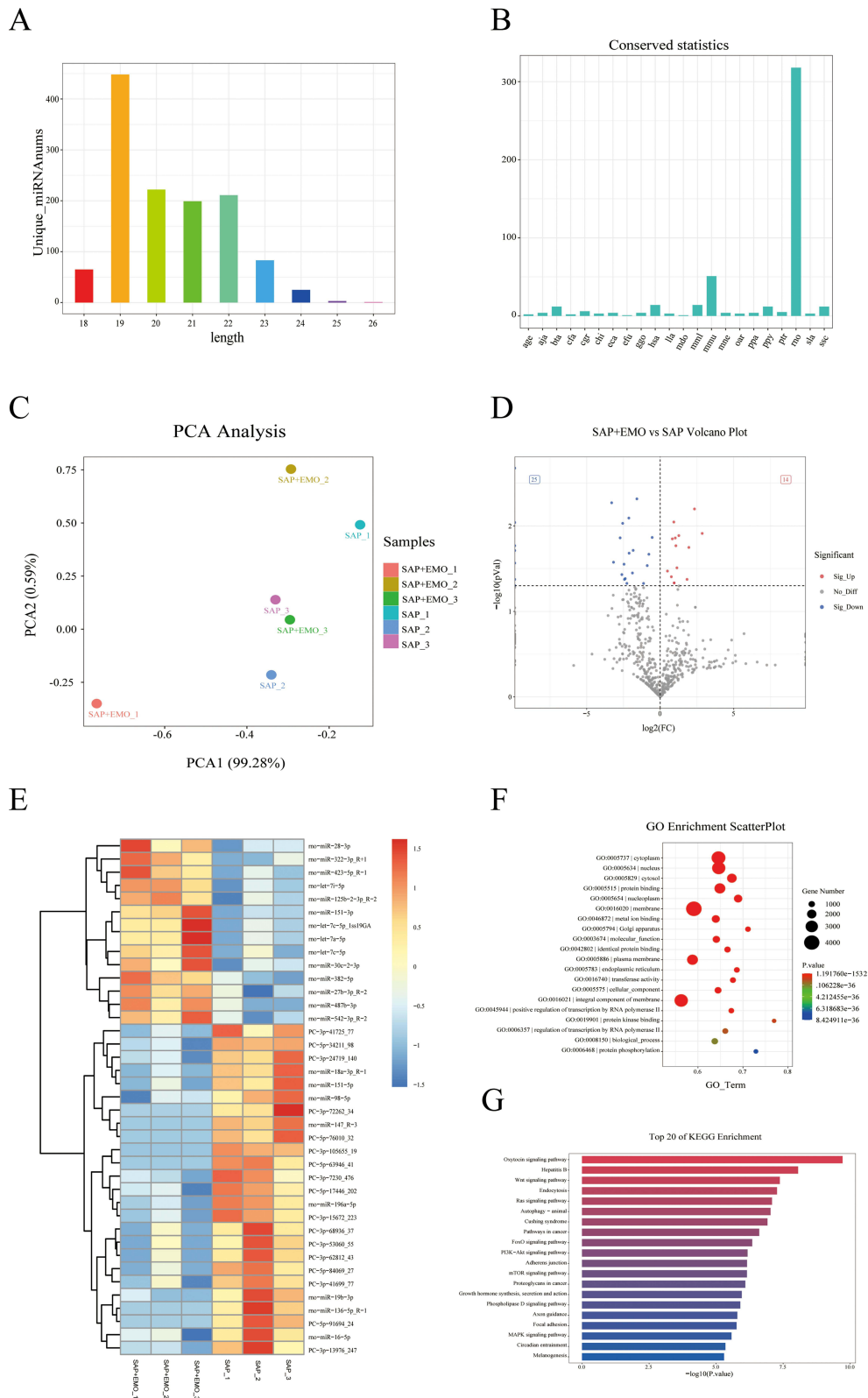


**Figure 6** miRNA sequencing and comprehensive analysis of plasma-derived exosomes. **(A and B)** The length and species conservative analysis of miRNAs. **(C)** Principal component analysis. Volcano plot of differentially expressed miRNAs (DEmiRNAs). **(E)** Clustering heat map of DE miRNAs. **(F)** GO functional enrichment analysis of DE miRNAs target genes. **(G)** KEGG functional enrichment analysis of DE miRNAs target genes.

miRanda to estimate the target genes of DEmiRNAs, respectively. The intersection of TargetScan and miRanda's prediction acts as the final target gene of DEmiRNAs. Figure 6F-G displays GO/KEGG enrichment analysis findings for potential target genes of DEmiRNAs.

## Verification of Significantly DEmiRNAs

To evaluate the repeatability of miRNA sequencing findings, we conducted a qRT-PCR analysis to detect the expression of miRNAs that exhibited the most significant differences in plasma/BALF-derived Exos. The statistical results were in agreement with the sequencing data. In contrast to the SAP group, EMO exhibited an up-regulation in the expression of NOVEL-rno-miR-29a-3p and rno-miR-300-3p in Exos derived from BALF. The down-regulation of rno-miR-653-3p and rno-let-7a-5p was observed, as depicted in Figure 7A. In comparison to the SAP group, the expression of rno-miR-487b-3p in Exos derived from plasma was up-regulated by EMO. The down-regulation of rno-miR-18a-3p was observed, as depicted in Figure 7B.

## EMO Partially Relies on NOVEL-Rno-miR-29-3p Upregulation to Protect Against SAP-Induced ALI

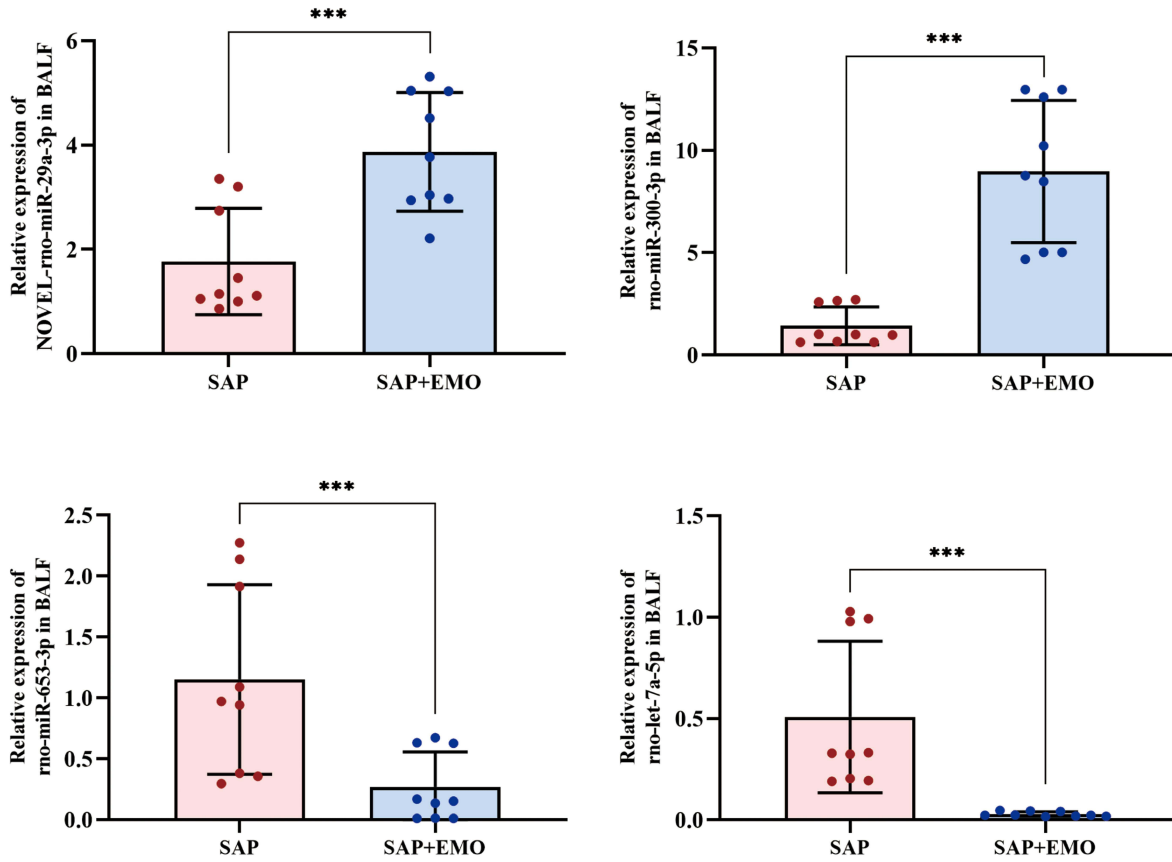
Since the therapeutic efficacy of BALF-SAP+EMO-Exo was superior to that of plasma-SAP+EMO-Exo, we concentrated on NOVEL-rno-miR-29a-3p, which is substantially upregulated in BALF-derived Exos. We synthesized antago-NOVEL-rno-miR-29a-3p and -NC. The experimental design and animal care are illustrated in Figure 8A. As shown in Figure 8B-E, EMO significantly improved lung injury, pulmonary edema, and respiratory dysfunction. Figure 8B-E demonstrates that antago-NOVEL-rno-miR-29a-3p partially reversed EMO's protective effect. These findings suggest that EMO may partly rely on NOVEL-rno-miR-29p-3p expression to prevent pulmonary injury in SAP rats.

## Discussion

Numerous research groups have provided evidence of the therapeutic efficacy of EMO in treating SAP. In 2005, Zhang et al<sup>15</sup> documented the advantageous effects of combining EMO and baicalein in suppressing pancreatic injury and inflammation in rats with SAP. Subsequent preclinical investigations have confirmed the protective properties of EMO against SAP-induced various conditions, including intestinal barrier dysfunction,<sup>16</sup> liver injury,<sup>17</sup> lung injury,<sup>11,18</sup> and systemic inflammatory response.<sup>19,20</sup> Our study also validated the therapeutic efficacy of EMO on SAP rats. The administration of EMO demonstrated a mitigating effect on the pathological damage inflicted on the pancreas and lungs by STC. Neutrophils are the primary effector cells that damage the pancreas and lungs during SAP. After the occurrence of SAP, circulating monocytes migrate and aggregate into pancreas and lung tissues and differentiate into M1 macrophages to release a high amount of inflammatory mediators, causing tissue damage. The quantity of M1-type macrophages often determines the progression and severity of inflammation. We found that EMO exhibited inhibitory properties against the migration of neutrophils and macrophages to the pancreas and lungs. Previously, Hu et al<sup>12</sup> found that plasma-SAP+EMO-Exo has the potential advantage of reducing lung damage in rats, and the mechanism may be associated with suppressing the release of pancreatic Exos and modifying the protein composition of plasma-derived Exos. However, the potential impact of EMO on SAP through modulation of humoral exosome-specific miRNAs remains unclear.

Exos are EVs that exhibit a particle size within the 30 to 150 nm range. Nearly all types of cells can actively secrete Exos. In a previously published review, we elucidated the ambivalent function of exosome-specific miRNAs in acute pancreatitis, which can be likened to a double-edged sword.<sup>6</sup> Following the onset of SAP, it has been observed that inflammatory cells, including macrophages and neutrophils, can release exosome-specific inflammatory miRNAs. This release can damage the pancreas and exacerbate dysfunction in extrapancreatic organs such as the intestine and lungs.<sup>21,22</sup> Conversely, specific parenchymal cells, namely pancreatic acinar cells and intestinal epithelial cells, can secrete Exos containing anti-inflammatory miRNAs, which combat inflammation and facilitate the mending of tissue injuries.<sup>23,24</sup> The secretion of exosome-specific inflammatory miRNAs by inflammatory cells and exosome-specific anti-inflammatory miRNAs by parenchymal cells is only sometimes definitive, and their functions may occasionally be

A



B

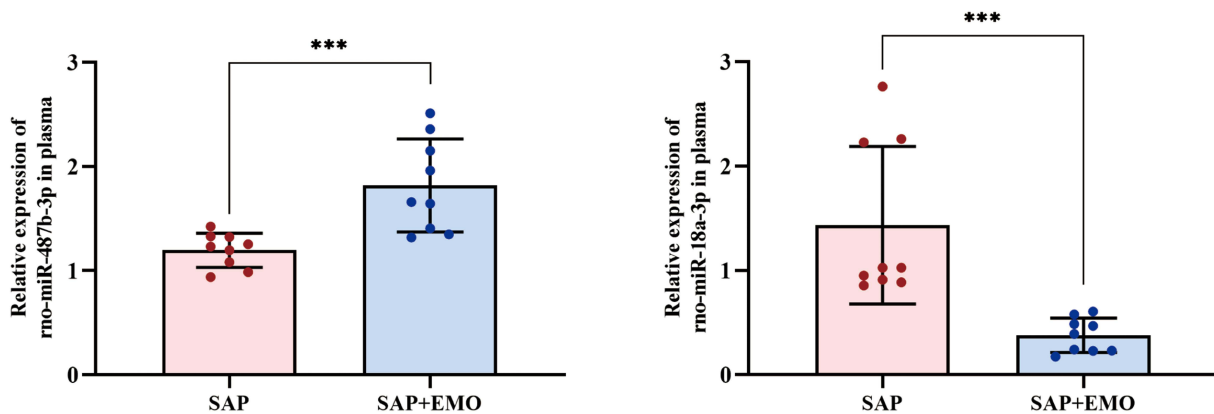


**Figure 7** Verification of significantly DE miRNAs. (A) The expression of NOVEL-rno-miR-29a-3p, rno-miR-300-3p, rno-miR-653-3p, and rno-let-7a-5p in exosomes derived from BALF. (B) The expression of rno-miR-487b-3p and rno-miR-18a-3p in exosomes derived from plasma. The data are presented as mean ± standard deviation of each group from three separate experiments. \*\*\* denotes p-value < 0.001.

interchanged. Tang et al<sup>25</sup> discovered that miR-183-5p, specific to EVS and derived from acinar cells, can induce macrophage polarization towards M1. This is achieved through the inhibition of forkhead box transcription factor O1 (FoxO1) expression, which ultimately exacerbates the severity of SAP. The utilization of Exo-specific miRNAs exhibits promising potential for the timely detection of SAP. Proteins and miRNAs that are specific to Exos and have been extracted from the urine, blood, and ascites of patients with SAP have the potential to serve as innovative biomarkers for evaluating the severity of SAP, as indicated by sources.<sup>26–28</sup> Exos have been utilized for therapeutic purposes through various methods, such as isolating Exos derived from stem cells or plants, manipulating the protein and nucleic acid

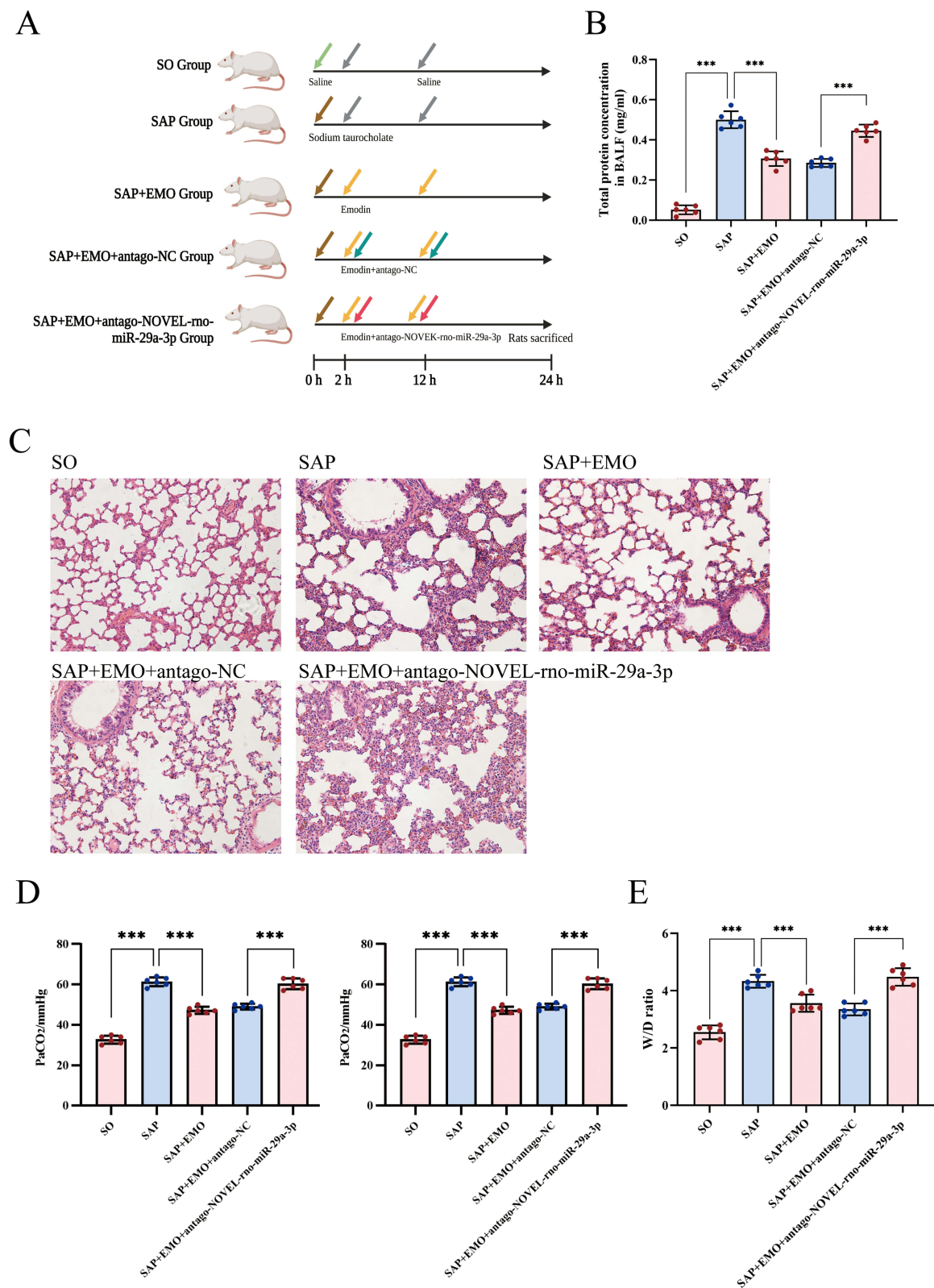


**Figure 8** EMO relies on NOVEL-rno-miR-29-3p upregulation to protect against SAP-induced ALI. **(A)** The experimental design and animal treatment. Created with BioRender.com. **(B)** Total protein concentration in bronchoalveolar lavage fluid. **(C)** HE staining of lung tissue sections (scale bar = 50  $\mu$ m). **(D)** Arterial blood gas analysis. **(E)** Wet-dry ratio of rat lung tissue. The data consisted of representative images from a minimum of three independent experiments or were presented as mean  $\pm$  standard deviation of each group ( $n = 6$ ). \*\*\* denotes  $p$ -value  $< 0.001$ .

content of exosomes, and applying exosomes for drug delivery. Han et al<sup>29</sup> discovered that using exosomes from mesenchymal stem cells of human umbilical cords effectively promoted pancreatic restoration in rats afflicted with traumatic pancreatitis. The study conducted by Chen et al<sup>30</sup> revealed that Exos obtained from mesenchymal stem cells had a notable impact on myocardial injury by activating antioxidant signaling pathways. In addition, using bone marrow/adipose-derived stem cells has demonstrated remarkable potential in managing sepsis-induced lung injury in the instance of ALI, as evidenced by studies.<sup>31–33</sup> However, the investigation into the modulation of protein and nucleic acid profiles conveyed by Exos for managing inflammatory disorders has been limited. Previous studies have demonstrated that EMO can effectively hinder inflammation and lung damage caused by SAP by regulating exosomal long non-coding RNA and protein profiles.<sup>12,34</sup> Our study revealed that administering plasma/BALF-SAP-Exo exacerbates lung injury induced by SAP in rats. Conversely, administering plasma/BALF-SAP+EMO-Exo ameliorates lung injury and suppresses the inflammatory response in SAP-induced rats. The cargo of Exos originating from plasma indicates the dynamic alterations occurring in bodily tissues and organs, whereas BALF is limited to the lungs. The changes in BALF-exosome cargo are more indicative of pathological alterations in the lungs. The results of our study indicate that SAP rats treated with Exos derived from BALF exhibited a more potent therapeutic response than those treated with Exos derived from plasma.

To investigate the mechanism by which EMO exerts its anti-inflammatory effects via Exos, we conducted a miRNA sequencing analysis of Exos derived from plasma/BALF. The miRNA expression profile of plasma and BALF-derived Exos in SAP rats underwent significant changes upon exposure to EMO. In particular, 34 DE miRNAs were detected when comparing BALF-SAP+EMO-Exo and BALF-SAP-Exo. qRT-PCR was employed to detect the expression of DE miRNAs exhibiting the most notable variations between the two groups. EMO elicited an up-regulation in the expression of NOVEL-rno-miR-29a-3p, NOVEL-rno-miR-15a-3p, and rno-miR-300-3p in Exos derived from BALF. Down-regulation of rno-miR-653-3p and rno-let-7a-5p expression in BALF-derived Exos was observed after EMO treatment. MiR-15 exhibits properties that suggest it possesses anti-inflammatory activity. Zhen et al<sup>35</sup> have previously reported that baicalin can increase the expression of miR-15a, which in turn can suppress the c-Jun-N-terminal kinase (JNK) signaling pathway, thereby reducing the incidence and progression of AP. Additionally, miR-15a inhibits macrophage activation stimulated by lipopolysaccharide (LPS)/interferon.<sup>36</sup> Thus, it is plausible that miR-15a plays a pivotal role in the anti-inflammatory mechanism of action of EMO. On the other hand, a comprehensive total of 39 DE miRNAs were detected when comparing plasma-SAP+EMO-Exo to plasma-SAP-Exo. qRT-PCR was utilized to identify DE miRNAs exhibiting the highest degrees of variance in Exos derived from plasma. EMO elicited an up-regulation in the expression of rno-miR-487b-3p, rno-miR-382-5p, and rno-miR-542-3p in Exos derived from plasma while causing a down-regulation in the expression of rno-miR-196a-5p and rno-miR-18a-3p in Exos derived from plasma. A previous study found a decrease in the expression of miR-382-5p in lung inflammation induced by exposure to particulate matter. Upregulation of miR-382-5p can effectively mitigate the overexpression of chemokine (C-X-C motif) ligand 12 (CXCL12), matrix metalloproteinase-9 (MMP9), and pro-inflammatory factors caused by exposure to particulate matter, thereby ameliorating lung damage.<sup>37</sup> In addition, we conducted a comparative analysis of the impact of EMO on miRNA expression profiles of Exos derived from plasma and BALF. The results revealed the presence of three shared DE miRNAs, namely rno-miR-19b-3p, rno-miR-98-5p, and rno-let-7a-5p. Of the three, the expression trend of rno-miR-98-5p remained consistent, wherein EMO exhibited a down-regulation of its expression. The purported function of miR-98-5p in the context of inflammation presents an apparent paradox. One possible effect of down-regulating miR-98-5p expression is the induction of M2-type polarization in macrophages, which may alleviate inflammation.<sup>38</sup> The administration of LPS elicits an increase in the expression of miR-98-5p in macrophages. Suppression of miR-98-5p expression impedes the activation of the nuclear factor kappaB (NF-κB) pathway and mitigates the inflammatory response. In contrast, it has been observed that suppression of miR-98-5p expression in ALI could potentially exacerbate the lung inflammation induced by LPS.<sup>39</sup> Hence, there is a potential for further investigation into the involvement of miR-98-5p in the pathogenesis of SAP-ALI and the regulatory mechanism of EMO.

The therapeutic efficacy of BALF-SAP+EMO-Exo in treating ALI appears to surpass that of plasma-SAP+EMO-Exo. This leads us to hypothesize that the notably upregulated miRNA, NOVEL-rno-miR-29a-3p, induced by EMO, maybe the key molecule responsible for its anti-inflammatory properties. The protective properties of miR-29a-3p are widely recognized in academic circles. Multiple investigations have demonstrated the potential capacity of miR-29a-3p

in mitigating colitis,<sup>40</sup> myocardial ischemia-reperfusion injury,<sup>41</sup> and endothelial dysfunction.<sup>42</sup> Myocardial injury in patients with SAP is infrequent, yet it can result in fatal consequences. Utilizing mesenchymal stem cell-derived extracellular vesicles containing miR-29a-3p exhibits promising therapeutic potential for treating myocardial injury associated with SAP. MiR-29a-3p can potentially hinder the activation of the toll-like receptor 4 (TLR4) signaling pathway by suppressing the expression of high mobility group box-1 (HMGB1), which can mitigate inflammation and myocardial damage.<sup>43</sup> The protective role of miR-29a-3p in ALI has been recently uncovered. The study conducted by Cui et al<sup>13</sup> revealed a significant down-regulation of miR-29a-3p in the plasma of patients with ARDS and the lung tissue of mice with ALI. Subsequently, the ALI mice were subjected to intratracheal instillation of miR-29a-3p mimics, which significantly improved lung inflammation induced by LPS. The underlying mechanism of this effect may be attributed to the inhibition of PANoptosis in alveolar epithelial cells.<sup>13</sup> PANoptosis represents a newly discovered mechanism of regulated cell death. The inflammatory programmed death mode is initiated through crosstalk between pyroptosis, apoptosis, and necroptosis. MiR-29a-3p can impede ZBP1-mediated PANoptosis by specifically targeting tumor necrosis factor receptor 1 (TNFR1).<sup>13</sup> The NOVEL-rno-miR-29a-3p variant we have identified exhibits some dissimilarity from rno-miR-29a-3p in terms of its seed sequence. Specifically, the variant differs from rno-miR-29a-3p due to substitutions at the 8th and 22nd bases, where the 8th base is replaced by C instead of A, and the 22nd base is replaced by T instead of A. The downstream target gene differences may be impacted. The results of our experiments indicate that the NOVEL-rno-miR-29a-3p molecule we identified possesses anti-inflammatory properties and can potentially mitigate SAP-ALI.

## Conclusion

The findings of this investigation indicate that Exos obtained from plasma and BALF of rats with SAP treated with EMO have potential therapeutic benefits for ALI associated with SAP. The mechanism of action of EMO is observed to have a significant impact on the miRNA expression profile of Exo derived from plasma and BALF. In addition, our study indicates that BALF-SAP+EMO-Exo exhibited superior anti-inflammatory effects in SAP rats compared to plasma-SAP+EMO-Exo. The findings of the rescue experiment provide additional evidence supporting the notion that the NOVEL-rno-miR-29a-3p, specific to Exos and derived from BALF, playing a crucial role in the therapeutic efficacy of EMO.

## Abbreviation

EMO, emodin; SAP, severe acute pancreatitis; ALI, acute lung injury; Exo, exosome; STC, sodium taurocholate; BALF, bronchoalveolar lavage fluid; miRNA, MicroRNA; DE miRNAs, differentially expressed miRNAs; AP, Acute pancreatitis; SIRS, systemic inflammatory response syndrome; MODS, multiple organ dysfunction syndrome; EVs, extracellular vesicles; Exos, exosomes; HE, hematoxylin-eosin; IHC, immunohistochemistry; TNF- $\alpha$ , tumor necrosis factor- $\alpha$ ; IL-1 $\beta$ , interleukin-1 $\beta$ ; NC, negative control; iNOS, inducible nitric oxide synthase; TSG101, tumor susceptibility gene 101; SD, Sprague-Dawley; SO, sham-operated; HE, hematoxylin-eosin staining; W/D, wet-dry weight; PaO<sub>2</sub>, partial pressure of oxygen; PaCO<sub>2</sub>, partial pressure of carbon dioxide; BCA, bicinchoninic acid assay; TEM, transmission electron microscope; NTA, nanoparticle tracking analysis; PCA, principal component analysis; FC, fold change; GO, Gene Ontology; MF, molecular function; CC, cellular component; BP, biological process; KEGG:Kyoto Encyclopedia of Genes and Genomes; PVDF, polyvinylidene fluoride; LPS, lipopolysaccharide.

## Funding

This study was supported by National Natural Science Foundation of China (NO. 82074158 and 82274311), National Key R&D Program of China (NO. 2019YFE0119300), and Applied Basic Research Program of Liaoning Province (NO. 2023JH2/101300126).

## Disclosure

Graphical abstract is created using BioRender.com. The authors declare no conflicts of interest in this work.

## References

1. Zerem E, Kurtcehajic A, Kunosić S, Zerem Malkočević D, Zerem O. Current trends in acute pancreatitis: diagnostic and therapeutic challenges. *World J Gastroenterol.* 2023;29(18):2747–2763. doi:10.3748/wjg.v29.i18.2747
2. Kang H, Yang Y, Zhu L, et al. Role of neutrophil extracellular traps in inflammatory evolution in severe acute pancreatitis. *Chin Med J.* 2022;135(23):2773–2784. doi:10.1097/CM9.0000000000002359
3. Ge P, Luo Y, Okoye CS, et al. Intestinal barrier damage, systemic inflammatory response syndrome, and acute lung injury: a troublesome trio for acute pancreatitis. *Biomed Pharmacother.* 2020;132:110770. doi:10.1016/j.biopha.2020.110770
4. Lanyu Z, Feilong H. Emerging role of extracellular vesicles in lung injury and inflammation. *Biomed Pharmacother.* 2019;113:108748. doi:10.1016/j.biopha.2019.108748
5. Khalaj K, Figueira RL, Antounians L, Lauriti G, Zani A. Systematic review of extracellular vesicle-based treatments for lung injury: are EVs a potential therapy for COVID-19. *J Extracell Vesicles.* 2020;9(1):1795365. doi:10.1080/20013078.2020.1795365
6. Yang Q, Luo Y, Lan B, et al. Fighting Fire with Fire: exosomes and Acute Pancreatitis-Associated Acute Lung Injury. *Bioengineering.* 2022;9(11). doi:10.3390/bioengineering9110615
7. Hu Y, Yang L, Lai Y. Recent findings regarding the synergistic effects of emodin and its analogs with other bioactive compounds: insights into new mechanisms. *Biomed Pharmacother.* 2023;162:114585. doi:10.1016/j.biopha.2023.114585
8. Sharifi-Rad J, Herrera-Bravo J, Kamiloglu S, et al. Recent advances in the therapeutic potential of emodin for human health. *Biomed Pharmacother.* 2022;154:113555. doi:10.1016/j.biopha.2022.113555
9. Xiang H, Zhang Q, Qi B, et al. Chinese Herbal Medicines Attenuate Acute Pancreatitis: pharmacological Activities and Mechanisms. *Front Pharmacol.* 2017;8:216. doi:10.3389/fphar.2017.00216
10. Xu C, Luo Y, Ntim M, et al. Effect of emodin on long non-coding RNA-mRNA networks in rats with severe acute pancreatitis-induced acute lung injury. *J Cell Mol Med.* 2021;25(4):1851–1866. doi:10.1111/jcmm.15525
11. Xu C, Zhang J, Liu J, et al. Proteomic analysis reveals the protective effects of emodin on severe acute pancreatitis induced lung injury by inhibiting neutrophil proteases activity. *J Proteomics.* 2020;220:103760. doi:10.1016/j.jprot.2020.103760
12. Hu Q, Yao J, Wu X, et al. Emodin attenuates severe acute pancreatitis-associated acute lung injury by suppressing pancreatic exosome-mediated alveolar macrophage activation. *Acta Pharm Sin B.* 2022;12(10):3986–4003. doi:10.1016/j.apsb.2021.10.008
13. Cui Y, Wang X, Lin F, et al. MiR-29a-3p Improves Acute Lung Injury by Reducing Alveolar Epithelial Cell PANoptosis. *Aging Dis.* 2022;13(3):899–909. doi:10.14336/AD.2021.1023
14. Xu Q, Wang M, Guo H, et al. Emodin Alleviates Severe Acute Pancreatitis-Associated Acute Lung Injury by Inhibiting the Cold-Inducible RNA-Binding Protein (CIRP)-Mediated Activation of the NLRP3/IL-1 $\beta$ /CXCL1 Signaling. *Front Pharmacol.* 2021;12:655372. doi:10.3389/fphar.2021.655372
15. Zhang XP, Li ZF, Liu XG, et al. Effects of emodin and baicalein on rats with severe acute pancreatitis. *World J Gastroenterol.* 2005;11(14):2095–2100. doi:10.3748/wjg.v11.i14.2095
16. Ning JW, Zhang Y, Yu MS, et al. Emodin alleviates intestinal mucosal injury in rats with severe acute pancreatitis via the caspase-1 inhibition. *Hepatobiliary Pancreat Dis Int.* 2017;16(4):431–436. doi:10.1016/S1499-3872(17)60041-9
17. Wang G, Sun B, Gao Y, Meng QH, Jiang HC. The effect of emodin-assisted early enteral nutrition on severe acute pancreatitis and secondary hepatic injury. *Mediators Inflamm.* 2007;2007:29638. doi:10.1155/2007/29638
18. Xia XM, Wang FY, Wang ZK, Wan HJ, Xu WA, Lu H. Emodin enhances alveolar epithelial barrier function in rats with experimental acute pancreatitis. *World J Gastroenterol.* 2010;16(24):2994–3001. doi:10.3748/wjg.v16.i24.2994
19. Ni Q, Sun K, Chen G, Shang D. In vitro effects of emodin on peritoneal macrophages that express membrane-bound CD14 protein in a rat model of severe acute pancreatitis/systemic inflammatory response syndrome. *Mol Med Rep.* 2014;9(1):355–359. doi:10.3892/mmr.2013.1771
20. Wang GJ, Wang Y, Teng YS, et al. Protective Effects of Emodin-Induced Neutrophil Apoptosis via the Ca(2+)-Caspase 12 Pathway against SIRS in Rats with Severe Acute Pancreatitis. *Biomed Res Int.* 2016;2016:1736024. doi:10.1155/2016/1736024
21. Shao Y, Li Y, Jiang Y, Li H, Wang J, Zhang D. Circulating exosomal miR-155-5p contributes to severe acute pancreatitis-associated intestinal barrier injury by targeting SOCS1 to activate NLRP3 inflammasome-mediated pyroptosis. *FASEB J.* 2023;37(6):e23003. doi:10.1096/fj.202300237R
22. Wu XB, Sun HY, Luo ZL, Cheng L, Duan XM, Ren JD. Plasma-derived exosomes contribute to pancreatitis-associated lung injury by triggering NLRP3-dependent pyroptosis in alveolar macrophages. *Biochim Biophys Acta Mol Basis Dis.* 2020;1866(5):165685. doi:10.1016/j.bbdis.2020.165685
23. Guo Y, Cao F, Ding Y, Lu J, Liu S, Li F. Acinar Cells Derived Exosomes Alleviate the Severity of Acute Pancreatitis. *Discov Med.* 2021;31(163):95–105.
24. Park EJ, Shimaoka M, Kiyono H. Functional Flexibility of Exosomes and MicroRNAs of Intestinal Epithelial Cells in Affecting Inflammation. *Front Mol Biosci.* 2022;9:854487. doi:10.3389/fmolb.2022.854487
25. Tang DS, Cao F, Yan CS, et al. Acinar Cell-Derived Extracellular Vesicle MiRNA-183-5p Aggravates Acute Pancreatitis by Promoting M1 Macrophage Polarization Through Downregulation of FoxO1. *Front Immunol.* 2022;13:869207. doi:10.3389/fimmu.2022.869207
26. Carrascal M, Areny-Balagueró A, de-Madaria E, et al. Inflammatory capacity of exosomes released in the early stages of acute pancreatitis predicts the severity of the disease. *J Pathol.* 2022;256(1):83–92. doi:10.1002/path.5811
27. Zhu Q, Luo J, Li HP, et al. Robust Acute Pancreatitis Identification and Diagnosis: rAPIDx. *ACS Nano.* 2023;17(9):8564–8574. doi:10.1021/acsnano.3c00922
28. Qu Y, Ding Y, Lu J, et al. Identification of key microRNAs in exosomes derived from patients with the severe acute pancreatitis. *Asian J Surg.* 2023;46(1):337–347. doi:10.1016/j.asjsur.2022.04.032
29. Han L, Zhao Z, Chen X, et al. Human umbilical cord mesenchymal stem cells-derived exosomes for treating traumatic pancreatitis in rats. *Stem Cell Res Ther.* 2022;13(1):221. doi:10.1186/s13287-022-02893-1
30. Chen M, Chen J, Huang W, et al. Exosomes from human induced pluripotent stem cells derived mesenchymal stem cells improved myocardial injury caused by severe acute pancreatitis through activating Akt/Nrf2/HO-1 axis. *Cell Cycle.* 2022;21(15):1578–1589. doi:10.1080/15384101.2022.2057762

31. Shen W, Zhao X, Li S. Exosomes Derived from ADSCs Attenuate Sepsis-Induced Lung Injury by Delivery of Circ-Fryl and Regulation of the miR-490-3p/SIRT3 Pathway. *Inflammation*. 2022;45(1):331–342. doi:10.1007/s10753-021-01548-2
32. Zhang T, Lu L, Li M, et al. Exosome from BMMSC Attenuates Cardiopulmonary Bypass-Induced Acute Lung Injury Via YAP/ $\beta$ -Catenin Pathway: downregulation of Pyroptosis. *Stem Cells*. 2022;40(12):1122–1133. doi:10.1093/stmcls/sxac063
33. Shen K, Wang X, Wang Y, et al. miR-125b-5p in adipose derived stem cells exosome alleviates pulmonary microvascular endothelial cells ferroptosis via Keap1/Nrf2/GPX4 in sepsis lung injury. *Redox Biol*. 2023;62:102655. doi:10.1016/j.redox.2023.102655
34. Wen X, He B, Tang X, Wang B, Chen Z. Emodin inhibits the progression of acute pancreatitis via regulation of lncRNA TUG1 and exosomal lncRNA TUG1. *Mol Med Rep*. 2021;24(5). doi:10.3892/mmr.2021.12425
35. Zhen J, Chen W, Liu Y, Zang X. Baicalin Protects Against Acute Pancreatitis Involving JNK Signaling Pathway via Regulating miR-15a. *Am J Chin Med*. 2021;49(1):147–161. doi:10.1142/S0192415X21500087
36. Zhu QJ, Wang J, Li Y, Bai ZJ, Guo XB, Pan T. PRKCA Promotes Mitophagy through the miR-15a-5p/PDK4 Axis to Relieve Sepsis-Induced Acute Lung Injury. *Infect Immun*. 2023;91(1):e0046522. doi:10.1128/iai.00465-22
37. Zhang X, Zhang Y, Meng Q, et al. MicroRNA-382-5p is involved in pulmonary inflammation induced by fine particulate matter exposure. *Environ Pollut*. 2020;262:114278. doi:10.1016/j.envpol.2020.114278
38. Peng Y, Wang Q, Yang W, Yang Q, Pei Y, Zhang W. MiR-98-5p expression inhibits polarization of macrophages to an M2 phenotype by targeting Trib1 in inflammatory bowel disease. *Acta Biochim Pol*. 2020;67(2):157–163. doi:10.18388/abp.2020\_5152
39. Chen J, Liu Q, Ding Z, et al. LncRNA NEAT1 aggravates lipopolysaccharide-induced acute lung injury by regulating the miR-98-5p/TLR4 axis. *J Biochem Mol Toxicol*. 2021;35(12):e22927. doi:10.1002/jbt.22927
40. Fukata T, Mizushima T, Nishimura J, et al. The Supercarbonate Apatite-MicroRNA Complex Inhibits Dextran Sodium Sulfate-Induced Colitis. *Mol Ther Nucleic Acids*. 2018;12:658–671. doi:10.1016/j.omtn.2018.07.007
41. Tian R, Guan X, Qian H, et al. Restoration of NRF2 attenuates myocardial ischemia reperfusion injury through mediating microRNA-29a-3p/CCNT2 axis. *Biofactors*. 2021;47(3):414–426. doi:10.1002/biof.1712
42. Bai Y, Liu X, Chen Q, Chen T, Jiang N, Guo Z. Myricetin ameliorates ox-LDL-induced HUVECs apoptosis and inflammation via lncRNA GAS5 upregulating the expression of miR-29a-3p. *Sci Rep*. 2021;11(1):19637. doi:10.1038/s41598-021-98916-7
43. Ren S, Pan L, Yang L, et al. miR-29a-3p transferred by mesenchymal stem cells-derived extracellular vesicles protects against myocardial injury after severe acute pancreatitis. *Life Sci*. 2021;272:119189. doi:10.1016/j.lfs.2021.119189

International Journal of Nanomedicine

Dovepress

## Publish your work in this journal

The International Journal of Nanomedicine is an international, peer-reviewed journal focusing on the application of nanotechnology in diagnostics, therapeutics, and drug delivery systems throughout the biomedical field. This journal is indexed on PubMed Central, MedLine, CAS, SciSearch<sup>®</sup>, Current Contents<sup>®</sup>/Clinical Medicine, Journal Citation Reports/Science Edition, EMBase, Scopus and the Elsevier Bibliographic databases. The manuscript management system is completely online and includes a very quick and fair peer-review system, which is all easy to use. Visit <http://www.dovepress.com/testimonials.php> to read real quotes from published authors.

Submit your manuscript here: <https://www.dovepress.com/international-journal-of-nanomedicine-journal>